Tailoring Water-Based Graphite Conductive Ink Formulation for Enzyme Stencil-Printing

Marchianò, Verdiana; Tricase, Angelo; Caputo, Mariapia; Farinini, Emanuele; Leardi, Riccardo; Imbriano, Anna; Leech, Dónal; Kidayaveettil, Reshma; Gentile, Luigi; Torsi, Luisa; Macchia, Eleonora; Bollella, Paolo

Published in:
Chemistry of Materials

DOI:
10.1021/acs.chemmater.3c02229

Published: 01/01/2023

Document Version
Final published version

Document License
CC BY

CHEMISTRY OF MATERIALS

Open Access

pubs.acs.org/cm

Article

Tailoring Water-Based Graphite Conductive Ink Formulation for Enzyme Stencil-Printing: Experimental Design to Enhance Wearable Biosensor Performance

Published as part of Chemistry of Materials virtual special issue "In Honor of Prof. Elsa Reichmanis".

Verdiana Marchianò, Angelo Tricase, Mariapia Caputo, Emanuele Farinini, Riccardo Leardi, Anna Imbriano, Dónal Leech, Reshma Kidayaveettil, Luigi Gentile, Luisa Torsi,* Eleonora Macchia,* and Paolo Bollella*

Cite This: *Chem. Mater.* 2024, 36, 358−370

Read Online

ACCESS | Metrics & More | Article Recommendations | Supporting Information

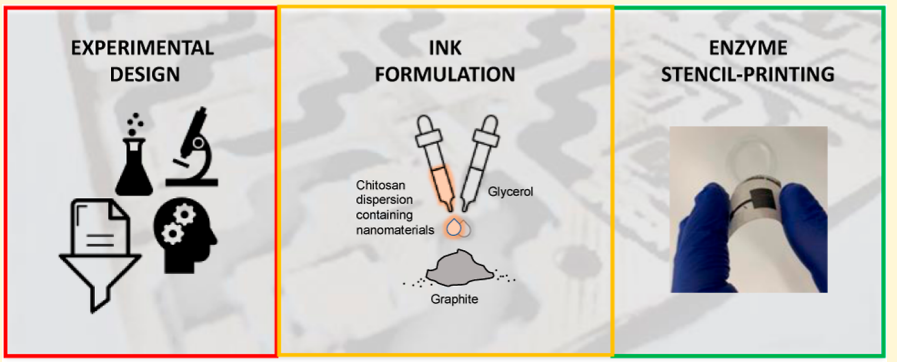

ABSTRACT: Herein, we report for the first time an experimental design-based approach to develop water-based graphite conductive ink containing enzymes and redox mediators to obtain fully printed wearable biosensors for lactate and glucose monitoring. The experimental design encompasses both electrochemical parameters, such as electroactive area and electron transfer rate constant, and rheological parameters, including elastic (G') and viscous (G'') moduli where G''/G' is expressed as tanδ. Notably, the printed electrodes exhibited an electroactive area A_{EA} of 3.95 ± 0.31 cm^2 and a roughness factor, ρ, of 43.8, which is 50 times higher than those of commercially available screen-printed electrodes. Furthermore, lactate oxidase and glucose oxidase are integrated within water-based graphite conductive ink to obtain enzyme-based inks: enzyme-ink (E-INK), to detect lactate, and enzyme mediator-ink (EM-INK), to detect glucose. The resulting biosensors demonstrated high sensitivity and low limit of detection 3.3 μA mM^{-1} and 0.3 ± 0.1 μM (ferricyanide as electron mediator), and 4.3 μA mM^{-1} and 3 ± 1 μM, for E-INK and EM-INK, respectively. The biosensors also exhibited excellent selectivity, maintaining their storage stability, with approximately 80−90% of the initial signal retained after 90 days. Overall, this promising system holds potential to be utilized as a flexible and wearable biosensor. Its use of biocompatible water-based inks makes it suitable for applications in sports medicine and remote clinical care.

KEYWORDS: *water-based conductive ink, modified electrodes, enzymes, stencil-printing*

1. INTRODUCTION

In recent years, there has been growing interest in the development of affordable wearable electrochemical biosensors for remote sensing. This has prompted researchers to explore new technological and research solutions aimed at reducing manufacturing costs and improving the reliability, reproducibility, and stability of these biosensing platforms.[1−4] One area of focus has been the search for novel materials and electrode preparation techniques that can address these challenges.[5−8]

Previously, conductive inks were primarily used for repairing electrical circuits and were expensive, requiring specific curing procedures involving lengthy preparation times and high temperatures.[9,10] Additionally, these inks were typically dispersed in organic solvents, which resulted in lower conductivities and the potential for poisoning biological

Received: August 31, 2023
Revised: November 21, 2023
Accepted: November 22, 2023
Published: December 27, 2023

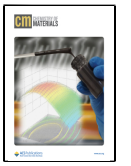

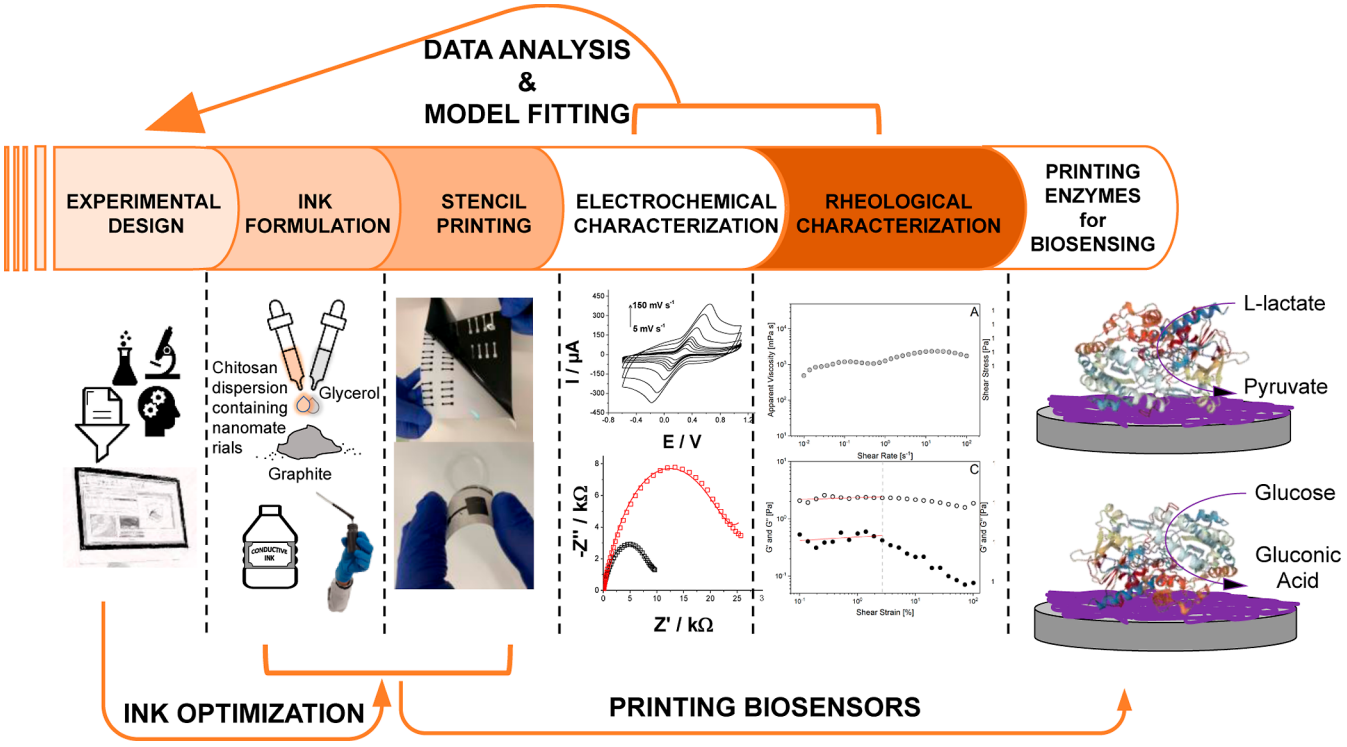

Figure 1. Scheme of the experimental design approach to develop enzyme stencil-printed biosensors.

recognition elements such as redox enzymes, antibodies, and DNA.[11−13] However, advancements in technology have led to the development of water-based lab-made inks, which offer comparable electrochemical performance to solid electrodes mentioned in the existing literature. This breakthrough has allowed for the construction of biosensor architectures with improved characteristics.[14−19]

To create reliable sensor devices, ink mixtures need to have a homogeneous composition and exhibit conductive properties, while also drying at a moderate pace.[20] Rapid drying can lead to surface cracks, which pose problems during electrode manufacturing, while slow drying hampers scalability and the ability to shape and size the electrodes accordingly.[12] Moreover, the use of water-based conductive inks has minimized the production of organic solvent waste, making a significant contribution to achieving zero eco-impact in the Point-of-Care biosensing market, a concern that has been emphasized during the COVID-19 pandemic.[1,21−23]

To ensure a high level of reproducibility and robustness, wearable enzyme-based biosensors need to be tested under real operating conditions, considering factors such as the blood/tissue or peripheral bodily fluid ratio, which can be influenced by various variables like hormonal dysfunctions, sweating rate, and age.[24,25] The immobilization of bioreceptors also plays a crucial role in achieving reproducibility and robustness. Notably, a significant advancement has been the ability to print enzymes directly onto a conductive support or embed them within a conductive ink.[26,27] This has become more achievable with the development of water-based conductive inks. Additionally, the roughness and porosity of the electrode surface can prevent enzyme denaturation, creating a diffusion barrier that reduces signal variation and minimizes the loss of enzymatic activity.[28]

Enzyme-based biosensors rely on redox enzymes that facilitate the catalytic oxidation/reduction of their substrates.[29−34] For instance, lactate biosensors often employ lactate oxidase from *Aerococcus viridans* (LOx) as the bioreceptor, while glucose biosensors commonly use glucose oxidase from *Aspergillus niger* (GOx). LOx contains flavin mononucleotide, which catalyzes the oxidation of lactate to pyruvate, accompanied by the reduction of O_2 to H_2O_2. Monitoring the electrochemical activity of both O_2 and H_2O_2 allows for an amperometric output proportional to lactate concentration.[35,36] However, concerns exist regarding the selectivity and reproducibility of results obtained from these first-generation lactate biosensors, primarily due to the high overpotential required for H_2O_2 oxidation/reduction and the fluctuation of O_2 levels in the solution as well as its limited availability in bodily fluids (0.22 mM). Similarly, GOx, which contains flavin adenine dinucleotide, catalyzes glucose oxidation and the simultaneous reduction of O_2 to H_2O_2.[30,37] Despite its previous reputation as an "ideal enzyme" among bioelectrochemists, GOx is now considered a reliable biocatalyst primarily for first- and second-generation biosensors, as it does not undergo direct electron transfer with electrodes.[38,39]

The development of conductive inks, which involves conductive materials, binders, and stabilizers, requires optimization of various processing variables to enhance their performance.[40] To this aim, a design of experiments (DoE) or experimental design multivariate approach based on a face-centered design was undertaken, allowing investigation of the interactions between these variables and their impact on the formulation.[41] Indeed, DoE allows for the evaluation of the effect of multiple independent variables on responses by simultaneously varying them in a reduced number of experiments.[42,43] As a result, a simple mathematical model could be obtained, relating the response with the experimental conditions, providing global knowledge in the whole experimental domain. This work reports for the first time an

https://doi.org/10.1021/acs.chemmater.3c02229
Chem. Mater. 2024, 36, 358−370

approach based on DoE to optimize the formulation of a water-based graphite conductive ink including graphite, chitosan, and glycerol as components. The ink formulation was optimized considering both electrochemical (e.g., electroactive area, electron transfer rate constant etc.) and rheological (e.g., the elastic modulus G', the viscous G'' moduli, etc.) parameters, as shown in Figure 1. Afterward, the optimized ink formulation was used to incorporate redox mediators and enzymes to fully print enzyme-based amperometric biosensors onto flexible supports. In particular, enzyme and enzyme/mediator inks were formulated to develop enzyme-based amperometric biosensors with several electronic configurations. The latter were further tested in model solutions to determine all analytical figures of merit, notably limit of detection (LOD), sensitivity, linear range, and so on. The proposed approach can be used to design a wide range of enzyme inks to develop reliable wearable enzyme-based amperometric biosensors that can be employed in remote personalized medicine.

2. EXPERIMENTAL SECTION

2.1. Chemicals and Reagents. The following chemicals and reagents were acquired from Merck Millipore (formerly Sigma-Aldrich) for use in the experiments: 4-(2-hydroxyethyl)piperazine-1-ethanesulfonic acid (HEPES), acetic acid (CH_3COOH), D-glucose, L-lactic acid, potassium chloride (KCl), potassium ferricyanide [$K_3Fe(CN)_6$], potassium ferrocyanide [$K_4Fe(CN)_6$], hydrochloric acid (HCl), sodium hydroxide (NaOH), uric acid, ascorbic acid, pyruvate, D-galactose, D-fructose, dopamine hydrochloride, isopropyl alcohol (IPA), graphite powder (<20 μm, synthetic), chitosan medium molecular weight, glycerol (ACS grade ≥ 99.5%), and glucose oxidase (GOx) from *A. niger*. Additionally LOx from *A. viridans* was obtained from Toyobo Enzymes. The LOx enzyme, with an activity of 300 U/mL, was dissolved in a phosphate buffer at pH 7.4, while GOx, also with an activity of 300 U/mL, was dissolved in a phosphate buffer at the same pH. Theosmium redox polymer (ORP), namely [Os(4,4′-dimethyl-2,2′-bipyridine)$_2$(poly vinylimidazole)$_{10}$Cl]$^{2+/+}$ (referred to as [Os(dmbpy)$_2$(Cl)(PVI)$_{10}$]), was synthesized as previously reported.[44] All solutions were prepared using Milli-Q water(18.2 MΩ cm, Millipore, Bedford, MA, USA).

2.2. Water-Based Conductive Ink Formulation. The water-based ink used in this study was created by using graphite, chitosan, and glycerol as the conductive material, binder, and stabilizer, respectively. To make the chitosan solution, 2.5% (w/v) chitosan was dissolved in 1 M acetic acid, and the solution was stirred at room temperature overnight. The chitosan solution was then further diluted to 1% w/v using distilled water, resulting in a final acetic acid concentration of 0.4 M. The water-based conductive ink was formulated according to the Experimental Design (Table 1 and Section 2.5). The SPG (stencil-printed graphite) electrodes were fabricated using poly(ethylene terephthalate) (PET) sheets that were cleaned with IPA and distilled water and then lightly sanded with fine emery paper (1500 grit) to enhance ink adhesion. A stencil was carved on a Smart Vinyl adhesive sheet using a Cricut Explore 3 with Design Space Software v.7.3.95.[18] Once the stencil was applied to the PET sheet, 500 μL of the conductive ink was placed on it and spread with a scraper. The prepared electrode was allowed to dry at room temperature for 10 min and then cured in an oven at 100 °C for 1 min. After curing, the stencil was peeled off, and the connecting track between the working electrode and the pad was insulated with a nail polish.[18] Enzyme-ink (E-INK) was formulated including LOx (1 mg/mL) within the optimized ink, while enzyme mediator-ink (EM-INK) was formulated including GOx (1 mg/mL) and Os(dmbpy)$_2$(Cl)-(PVI)$_{10}$ (0.5 mg/mL). Both the E-INK and EM-INK were allowed to cure at room temperature for 30 min. After curing, the stencil was peeled off, and the connecting track between the working electrode and the pad was insulated with nail polish.

Table 1. Experimental Matrix, Experimental Plan, and Responses of the Face-Centered Design for the Optimization of the Conductive Ink Formulation

run	X_1	X_2	graphite (%)	chitosan (%)	A_{EA} (cm^2)	k^0 (cm s^{-1}) (×10^{-3})	tan δ
1	0	0	90	1.8	1.33	9.67	2.93
2	−1	−1	85	1.5	1.45	3.88	3.26
3	0	0	90	1.8	2.28	8.99	3.28
4	1	1	95	2.1	1.57	6.23	2.86
5	1	−1	95	1.5	4.11	12.50	4.85
6	−1	1	85	2.1	0.89	5.71	6.00
7	0	0	90	1.8	1.54	2.26	4.04
8	−1	0	85	1.8	0.95	2.71	5.49
9	1	0	95	1.8	1.64	4.57	5.11
10	0	−1	90	1.5	3.15	9.46	4.14
11	0	1	90	2.1	1.87	3.99	4.26

2.3. Electrochemical Characterization. Cyclic voltammetry (CV), amperometry, and electrochemical impedance spectroscopy (EIS) experiments were conducted using a PalmSens4 electrochemical workstation equipped with PSTrace 5.6v software. All potential values mentioned in the paper are referenced to a BASi Ag|AgCl|KCl (3 M) electrode, and a platinum wire served as counter electrode. The working electrodes used were SPG electrodes, which had a geometric area of 9 mm^2 and a square shape with dimensions of 3 × 3 mm ($l \times l$). Additionally, DRP-C110 screen-printed electrodes were employed as working electrodes but solely for benchmarking purposes in terms of electroactive area (A_{EA}) and electron transfer rate constant (k^0).

2.4. Rheological Measurements. Rheological measurements were carried out using a stress-controlled rheometer Anton Paar MCR302e (Anton Paar Gmbh, Graz, Austria) equipped with a concentric cylinder geometry (inner diameter of 16.662 mm and a gap of 0.704 mm), also known as Taylor−Couette geometry. The temperature was controlled by a Peltier system (±0.01 °C), while a water bath was used as a reference for the Peltier. To prevent errors due to methanol evaporation, a solvent trap was surrounded the measuring geometry.

Stationary and small amplitude oscillatory shear measurements were performed on all investigated samples.[45] Flow curve experiments were conducted within a shear rate range of 10^{-2} to 10^{2} s^{-1} at a temperature of 25 °C. Prior to the flow curve, amplitude and frequency sweeps were carried out. Following the flow curve, a second frequency sweep was performed for all samples to assess the potential deformation effects.

The small amplitude dynamic tests provided information on the linear viscoelastic behavior of materials through the determination of the complex shear modulus

$$G^*(\omega) = G'(\omega) + iG''(\omega) \quad (1)$$

where $G'(\omega)$ is the storage or elastic modulus, and $G''(\omega)$ is the loss or viscous modulus. $G'(\omega)$ is a measure of the reversible, elastic energy, while $G''(\omega)$ represents the irreversible viscous dissipation of the mechanical energy.

The applied strain amplitude for the viscoelastic measurements was reduced until the linear response regime was reached. Such an analysis has been carried out by performing amplitude sweep tests in a strain range between 0.01 and 100%. The frequency sweep tests were performed between 0.2 and 100 rad/s. For simplicity in the text $G'(\omega)$ and $G''(\omega)$ will be indicated as G' and G''. If δ is the phase shift between the applied oscillatory deformation and the material response then, based on the trigonometric relationship, the loss factor is

$$\tan \delta = \frac{G''}{G'} \quad (2)$$

https://doi.org/10.1021/acs.chemmater.3c02229
Chem. Mater. 2024, 36, 358−370

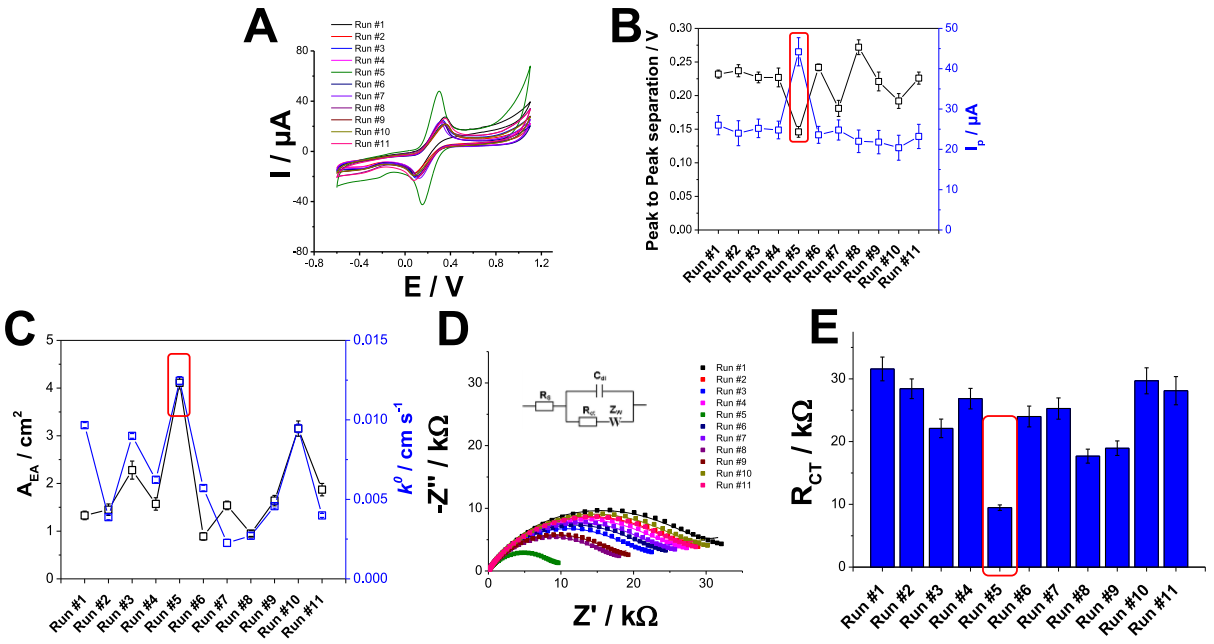

Figure 2. (A) CVs at 50 mV/s scan rate of SPG electrodes(inks: run #1 black, run #2 red, run #3 blue, run #4 magenta, run #5 olive, run #6 navy, run #7 violet, run #8 purple, run #9 wine, run #10 dark yellow and run #11 pink) recorded in 5 mM $Fe(CN)_6^{3-/4-}$ (prepared in 10 mM HEPES buffer pH 7.2 + 100 mM KCl); (B) peak-to-peak separations (black curve) and peak currents (blue curve) extracted from CVs at 50 mV/s for all formulated inks; (C) electroactive areas (black curve) and electron transfer rate constants (blue curve) extracted from CVs recorded at different scan rates (from 5 to 150 mV/s); (D) EIS curves recorded applying E = 0.23 V from 100 kHz to 0.1 Hz with amplitude 5 mV of SPG electrodes (inks: run #1 black, run #2 red, run #3 blue, run #4 magenta, run #5 olive, run #6 navy, run #7 violet, run #8 purple, run #9 wine, run #10 dark yellow and run #11 pink) in 5 mM $Fe(CN)_6^{3-/4-}$ (prepared in 10 mM HEPES buffer pH 7.2 + 100 mM KCl); (E) R_{CT} extracted by using Randles equivalent circuit for all SPG electrodes.

2.5. Experimental Design. A two-factor face-centered design, with the experimental matrix reported in Table 1, was developed to optimize the stencil-printed electrode ink formulation. The factors examined were the percentage of graphite with respect to glycerol (X_1), and the percentage of chitosan (X_2). The explored ranges were between 85% (with 15% glycerol) and 95% of graphite (with 5% glycerol) and 1.5 and 2.1% of chitosan. This domain was settled to explore the typical range of experimental conditions for water-based formulation of conductive inks.[18] The resulting experimental matrix is shown in Table 1. The measured responses were the electroactive area (A_{EA}), the electron transfer rate constant (k^0), and the rheological parameter tan $\delta = \frac{G''}{G'}$, obtained from the electrochemical and rheological characterizations (vide supra) of the water-based inks. All of the responses should be maximized. The responses for each condition of the experimental plan were assessed from two repeated measurement and the average response is reported in Table 1. For each response, the analytical variability was computed as pooled standard deviation, being 0.12 cm^2 for the A_{EA}, 0.019 × 10^{-3} cm s^{-1} for k^0, and 0.45 for tan δ, with 11 degrees of freedom. The experiments were conducted in random order not to introduce unwanted systematic effects. The models were computed by multilinear regression using CAT (Chemometric Agile Tool) open-source software,[46] with five degrees of freedom.[41] Statistical significance was set as customary at a confidence level of p = 0.05. The experimental variability was evaluated as the standard deviation. Therefore, the experimental variability is 0.50 cm^2 for the A_{EA}, 4.10 × 10^{-3} cm s^{-1} for k^0, and 0.57 for tan δ, meaning that for the first two responses the experimental variability is significantly larger than the analytical variability.

3. RESULTS AND DISCUSSION

3.1. Electrochemical Characterization of Stencil-Printed Graphite Electrode. The graphite printed electrodes were prepared using stencil-printing of water-based graphite conductive inks onto flexible PET, as described previously. The composition of the electrodes was formulated according to the face centered design as reported in Table 1 and electrode responses characterized using CV with 5 mM $Fe(CN)_6^{3-/4-}$ at various scan rates ranging from 5 to 150 mV s^{-1} (data not shown).[47] From the CV measurements at 50 mV s^{-1}, reported in Figure 2A the SPG electrodes exhibited different peak-to-peak separations and peak currents (Figure 2B black and blue curves, respectively). In particular, electrodes with lower content of graphite (run #2, run #6 and run #8) reported a higher peak-to-peak separation, notably 0.237 ± 0.009, 0.242 ± 0.005 and 0.272 ± 0.011 V, and a lower peak current, notably 24.0 ± 3.5, 23.6 ± 2.1 and 22.0 ± 2.8 μA. Both parameters can be associated with higher electrical resistance of the ink formulation and lower conductivity once cured. Based on these parameters, run #5 reported the lowest peak-to-peak separation (0.146 ± 0.008 V) and the highest peak current of (44.2 ± 3.5 μA). Figure 2C reports the electroactive areas (A_{EA}) for all formulated inks calculated by using Randles−Ševčík equation (black curve)[47] and the electron transfer rate constant (blue curve) calculated by using a mixed model based on an extended method merging the Klingler−Kochi and Nicholson and Shain methods.[48] Run #5 ink reported the highest A_{EA}, notably 4.11 ± 0.13 cm^2, and an electron transfer rate constant (k^0) of (12.5 ± 0.3) × 10^{-3} cm s^{-1} (Figure 2C). Considering a geometric area (A_{GEO}) of 0.09 cm^2, the roughness factor (ρ) was calculated as 45.6. Additionally, all electrodes were analyzed through EIS to determine the resistance to the charge transfer (R_{CT}) of a redox molecule, which can be extrapolated by using the Randles equivalent circuit (Figure 2D,E). All extracted data from the fitting are reported in Table S1 (Supporting

https://doi.org/10.1021/acs.chemmater.3c02229
Chem. Mater. 2024, 36, 358−370

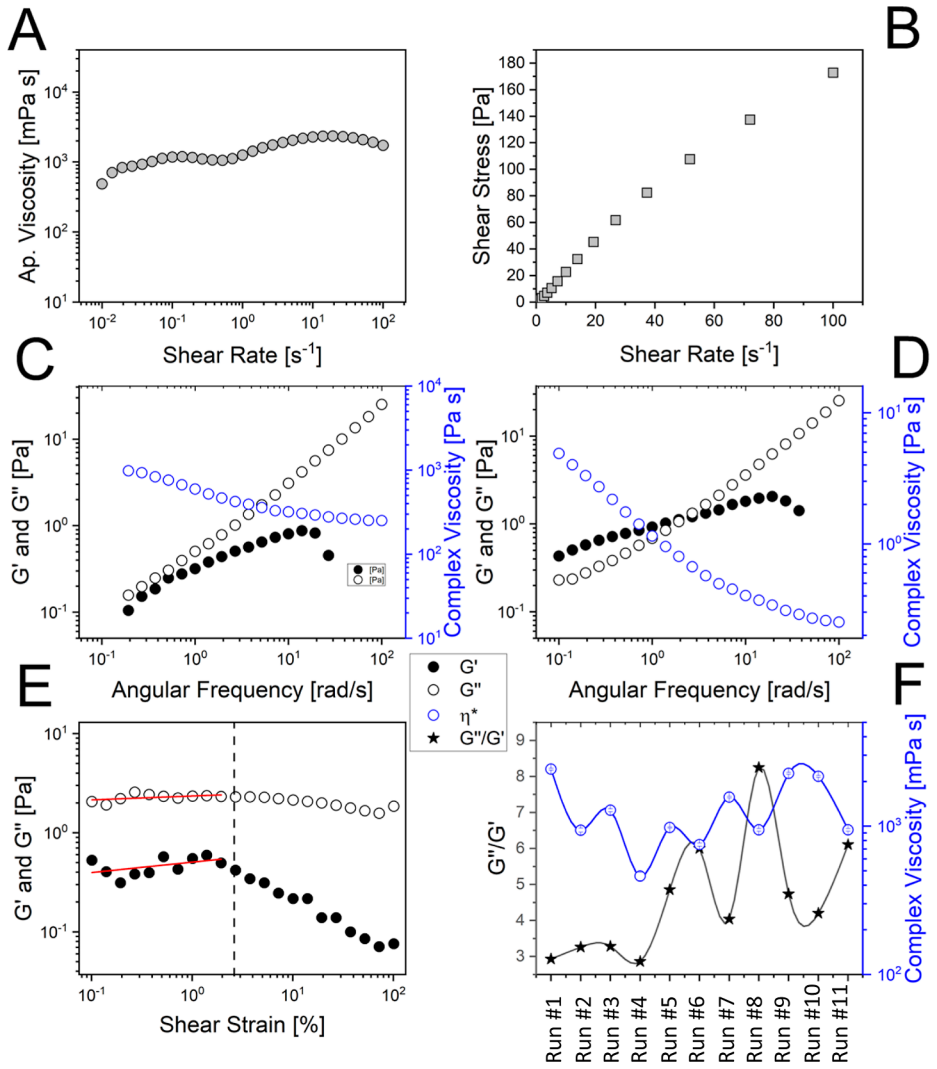

Figure 3. Flow curve of run #5 illustrates the relationship between apparent viscosity (A) and shear stress (B) with respect to the shear rate. Additionally, the frequency sweep (C), carried out at a shear strain of 0.01%, reveal the behavior of the elastic modulus, G', and viscous modulus, G'', respectively, in relation to angular frequency; frequency sweep experiment performed after flow curve for the system run #5 at 25 °C (D); the amplitude sweep test performed before the flow curve at an angular frequency of 10 rad/s used to extract tan δ in the linear viscoelastic regime (E). In the amplitude sweep, the red line represents a linear fit used to determine G' and G' at low strain and angular frequency; G''/G' and complex viscosity for all investigated samples at 25 °C; (F). All experiments are performed at a temperature of 25 °C.

Information). All ink formulations showed R_{CT} ranging between 15 and 30 kΩ, except for run #5 electrodes that reported an R_{CT} of 9.5 ± 0.4 kΩ due to high graphite and low binder contents, which are positively affecting the electrochemical performance of printed electrodes as previously reported.

3.2. Rheological Characterization of Formulated Water-Based Graphite Ink. Most printing inks consist of solid pigment particles suspended in complex vehicles. Traditional oleoresinous oil-based vehicles have been replaced to some extent by heatset inks (resins dissolved in petroleum solvents), flexographic inks (resins in alcohol), and steamset inks (resins in glycols). Latexes are becoming less common, while plastisols are also being considered. When solid particles such as pigments or extenders are added to a vehicle to create a commercially valuable product, it consistently leads to non-Newtonian, generally to nonlinear flow behavior. Consequently, the flow of ink becomes more challenging to describe and understand compared with the flow of pure liquids. The flow curve of the inks strictly depends on their formulation used in various applications: screen printing, gravure printing, inkjet printing and spray coating.[49] Inks can show a variety of behavior under flow, and consequently they can be classified as pseudoplastic (shear-thinning), yield-pesudoplastic (shear-thinning after reaching the yield stress), or quasi-Newtonian. The quasi-Newtonian behavior is due to the stress-versus-shear rate curve that is linear only within the shear rate range of 50−500 s^{-1}. Below this range, the curve shows a distinct curvature toward the origin.[49] In our formulation, chitosan was incorporated as a binder in the graphite suspension. The presence of chitosan can induce a viscoelastic response. Specifically, hydrophobic interactions between chitosan chains can lead to a sol−gel transition, resulting in gel formation depending on pH and concentration.[50] Chitosan is commonly employed in conjunction with other polymers to create composites for controlled release purposes.[51] In our case, all systems demonstrate quasi-Newtonian behavior, as illustrated in Figure 3 for run #5. Specifically, the flow curve demonstrates

https://doi.org/10.1021/acs.chemmater.3c02229
Chem. Mater. 2024, 36, 358−370

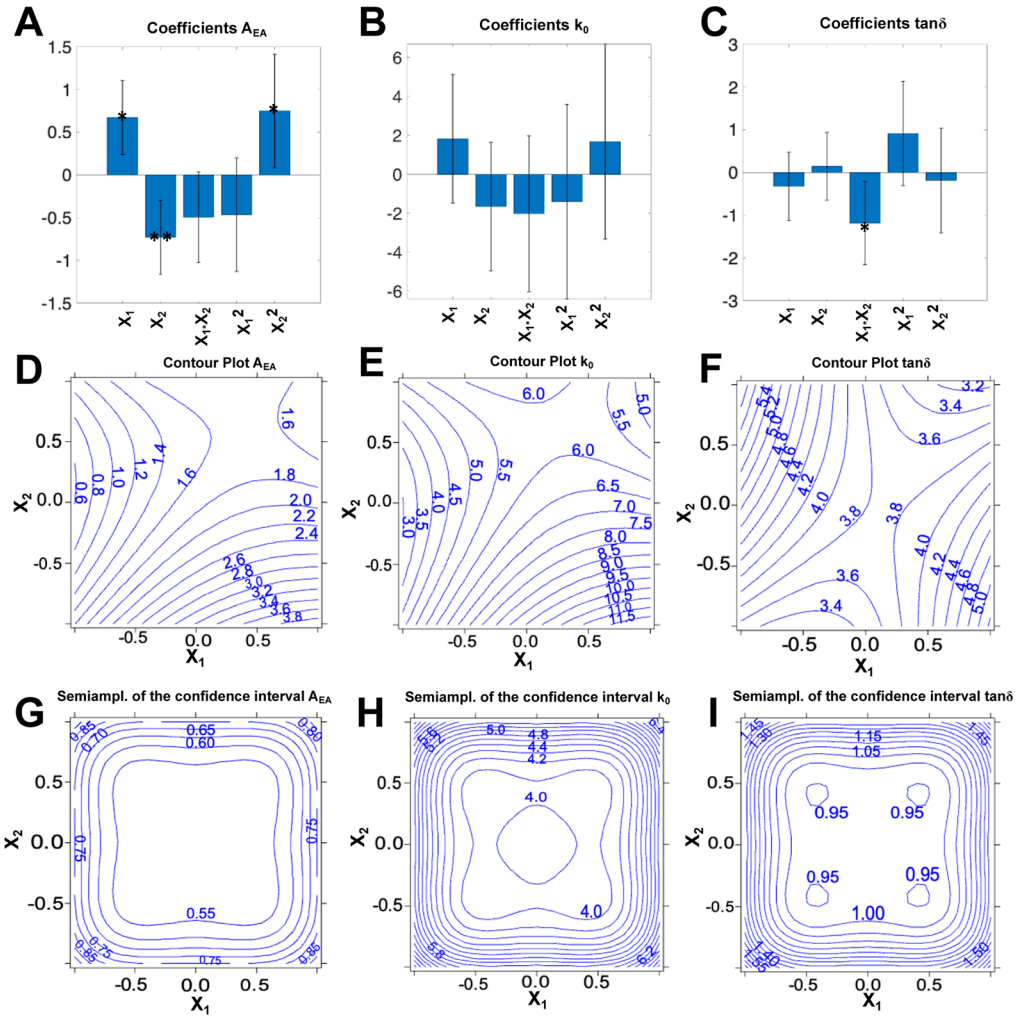

Figure 4. (A–C) Bar plot of the coefficients of the models of the three responses (the error bars correspond to the confidence intervals at $p = 0.05$; the stars indicate the significance of the coefficient (* = $p < 0.05$, ** = $p < 0.01$)); (D–F) contour plots of the responses; (G–I) contour plots of the semiamplitude of the confidence interval of the responses.

complex behavior at low shear rates but becomes Newtonian-like after 50 s^{-1} (Figure 3A,B). The frequency sweep measurement indicates a gradual shear-thinning effect as a function of the frequency (Figure 3C). However, the elastic modulus G' is consistently lower than the viscous modulus G'' across all investigated angular frequencies and shear strain ranges. Therefore, we classify the system as quasi-Newtonian. It is worth noting that the frequency sweep conducted after the flow curve (Figure 3D), for instance, after deformation, exhibits a different behavior compared to the frequency sweep conducted before the flow curve (Figure 3C). This discrepancy suggests the presence of a potential out-of-equilibrium state, such as partial aggregation. Tan δ ($=G''/G'$) in the linear viscoelastic regime can be extracted from the amplitude sweep performed at an angular frequency of 10 rad/s (Figure 3E). Figure 3F presents the complex viscosity and the tan δ ($=G''/G'$), as defined in eq 2 for the corresponding samples. A minimum value of complex viscosity, along with a minimum tan δ, is observed at the highest graphite and chitosan content (run #4). Conversely, a maximum value of tan δ is observed for run #6. The intermediate sample, run #5, demonstrates the most favorable fit in terms of both complex viscosity and tan δ.

3.3. Experimental Design Applied to Water-Based Graphite Inks. The optimization of the ink formulation was accomplished with an Experimental Design approach, aiming at improving the electrochemical performance, namely, the electroactive area (A_{EA}) and the electron transfer rate constant (k^0), while maximizing tan δ, to improve the homogeneity of the stencil printed electrode. This will ensure the possibility to obtain a conductive ink with high electrochemical performance but also printable by using a stencil onto different types of flexible supports. To this aim, the percentage of graphite with respect to glycerol (X_1), and the percentage of chitosan (X_2), have been varied according to a face-centered design,[41] with the experimental matrix provided in Table 1. The number of experiments required by such a design is $2^k + 2{\cdot}k + n$, corresponding to the combination of a factorial design, a star design, and n replicates of the center point. In the specific case, with the number of variables $k = 2$ and the number of replicates of the center point $n = 3$, 11 experiments are required. While the experimental matrix is built up from the coded values, the experimental plan reports the real value of the variables used to fabricate the stencil printed electrodes. Thus, the water-based inks were formulated according to the conditions settled by the experimental plan and fully electrochemically and rheologically characterized, recording

https://doi.org/10.1021/acs.chemmater.3c02229
Chem. Mater. 2024, 36, 358−370

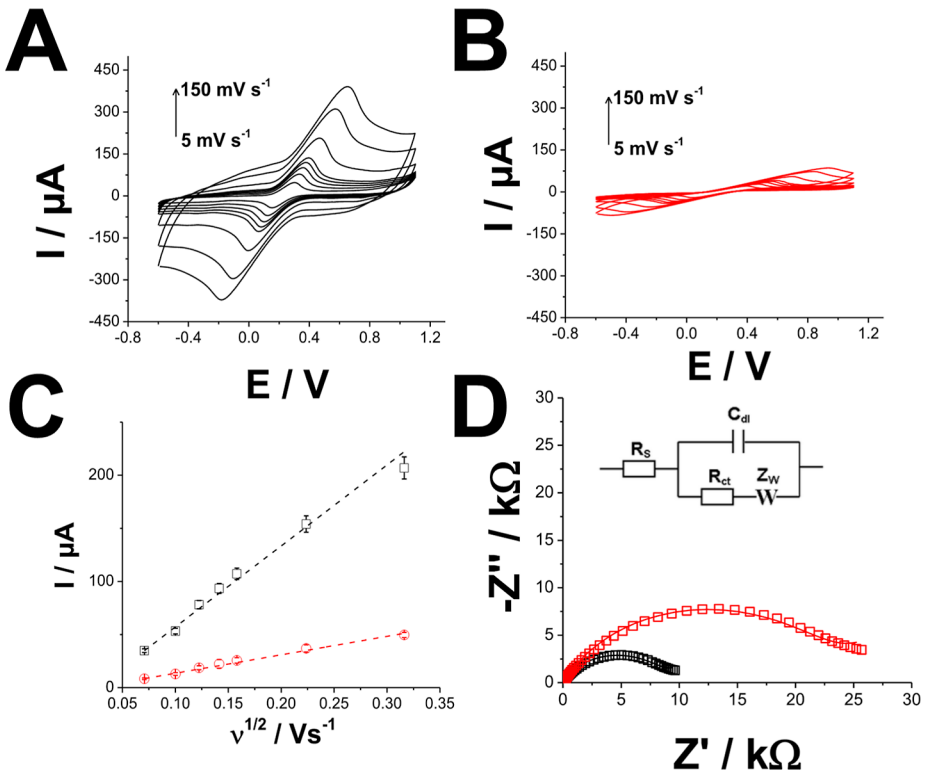

Figure 5. (A) CVs at different scan rates (5−150 mV/s) of optimized ink SPG electrodes recorded in 5 mM $Fe(CN)_6^{3-/4-}$ (prepared in 10 mM HEPES buffer pH 7.2 + 100 mM KCl); (B) CVs at different scan rates (5−150 mV/s) of DRP-110 screen printed electrodes recorded in 5 mM $Fe(CN)_6^{3-/4-}$ (prepared in 10 mM HEPES buffer pH 7.2 + 100 mM KCl); (C) slope i_p vs $\nu^{1/2}$ for optimized ink SPG electrodes (black curve) and DRP-110 screen printed electrodes (red curve) extracted from CVs recorded at different scan rates (from 5 to 150 mV/s); (D) EIS curves recorded applying E = 0.23 V from 100 kHz to 0.1 Hz with amplitude 5 mV of optimized ink SPG electrodes (black curve) and DRP-110 screen printed electrodes (red curve) in 5 mM $Fe(CN)_6^{3-/4-}$ (prepared in 10 mM HEPES buffer pH 7.2 + 100 mM KCl).

the responses, namely, A_{EA}, k^0, and tan δ. The experiments were performed in the randomized order reported in Table 1 to avoid introducing unwanted systematic effects. Based on those experiments, the following quadratic models have been obtained

$$A_{EA}=1.73 + 0.67X_1^{(*)}-0.73X_2^{(**)}-0.49X_1X_2-0.47X_1^2 +0.75X_1^{2(*)} \quad (3)$$

explaining 81.9% of the variance, with a standard deviation of the residuals of 0.41 cm^2

$$k^0(10^{-3})=6.19 + 1.83X_1-1.64X_2-2.02X_1X_2-1.40X_1^2 +1.69X_2^2 \quad (4)$$

explaining 13.1% of the variance, with a standard deviation of the residuals of 3.10 10^{-3} cm s^{-1}

$$\tan\delta = 3.80 - 0.32X_1+0.14X_2-1.18X_1X_2^{(*)}+0.91X_1^2 -0.18X_2^2 \quad (5)$$

with a 49.5% explained variance, and a standard deviation of the residuals 0.76. The standard deviations of the residuals of the three responses are in agreement with the experimental variability registered at the center point, meaning that no lack of fit is present. The coefficients of the A_{EA} and k^0 models are reported in Figure 4A−C as bar plots. The coefficients' significance level is indicated according to the usual convention, with *p < 0.05, **p < 0.01 and ***p < 0.001.

The incertitude of the prediction is provided in Figure 4D−I, where the contour plots of the semiamplitude of the confidence interval of the responses are plotted. For the first response, namely, A_{EA}, as suggested by the significance of the linear terms, increases with increasing graphite and decreasing chitosan. Furthermore, the significant quadratic term for chitosan indicates that the behavior is not linear. The model of the second response, k^0, explains only 13% of the variance and has no significant coefficients. Therefore, no information about the effect of the variables on this response can be obtained.

In the model for the rheological parameter tan δ response, the interaction between the two variables is the only significant coefficient. The response surface, depicted in Figure 4F, shows that an increase of graphite increases tanδ when the chitosan percentage is at the lower level, while it has the opposite effect when chitosan is at the higher level. On the other hand, an increase of chitosan increases the response when graphite is at the lower level, while it decreases the response when graphite is at the higher level. Therefore, the highest response is obtained with both variables at the higher level or both variables at the lower level, with the former condition to be preferred since it also corresponds to the highest predicted values for the electroactive area A_{EA} response. Therefore, from the analysis of the response surfaces, it is apparent that the condition corresponding to 95% graphite 5% glycerol and 1.5% chitosan (coded values +1, −1, corresponding to experiment 5 in Table 1) gives the highest predicted values for all the responses.

https://doi.org/10.1021/acs.chemmater.3c02229
Chem. Mater. 2024, 36, 358−370

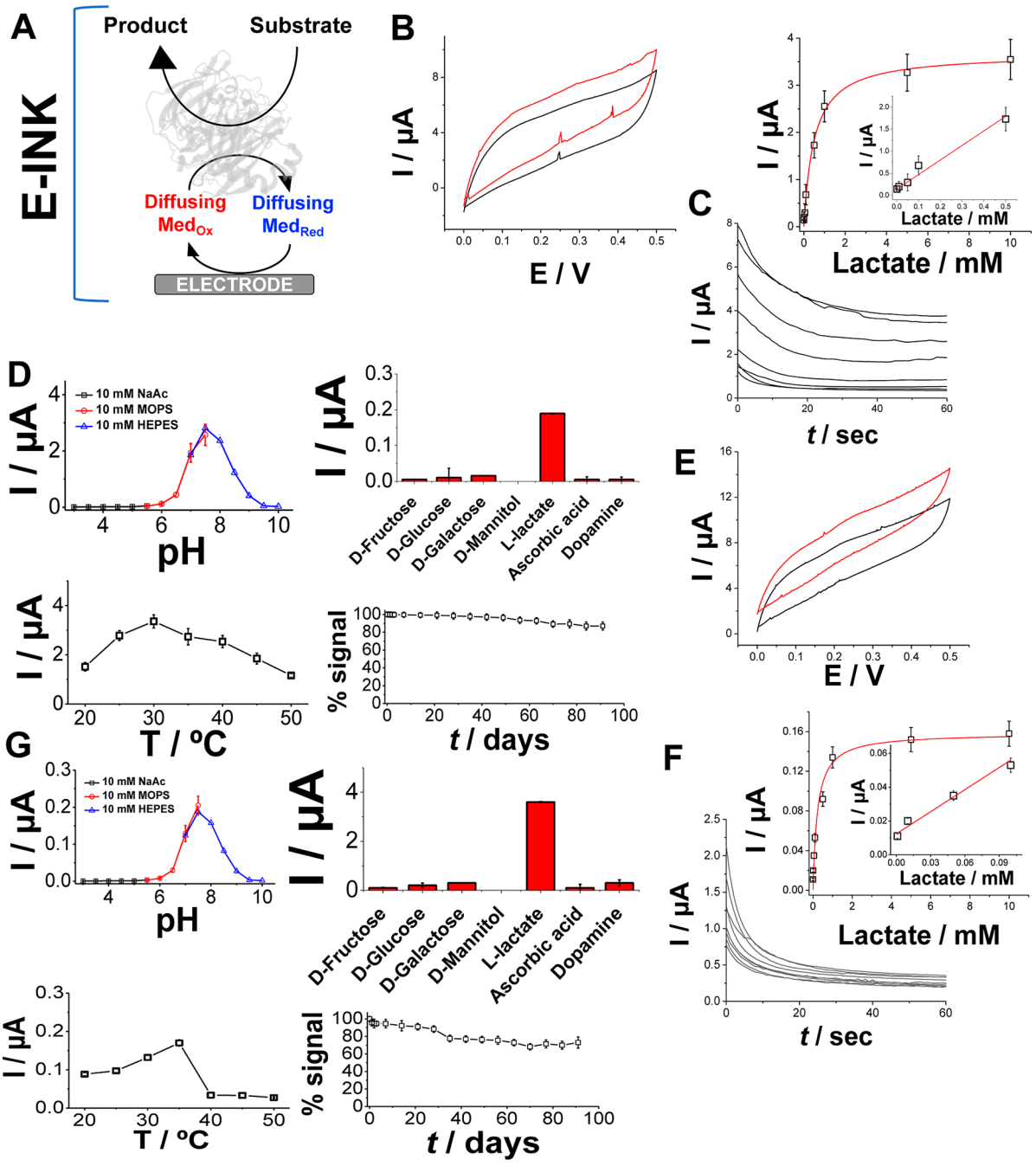

Figure 6. (A) Operating scheme of E-INK; (B) CVs for E-INK modified electrode in nonturnover (10 mM buffer pH 7.5 + 100 mM KCl + 125 μM ferricyanide, black curve) and turnover conditions (addition of 10 mM L-lactate, red curve), scan rate 5 mV s^{-1}; (C) amperometric measurements performed at E_{appl}: + 0.3 V for E-INK modified electrode in 10 mM buffer pH = 7.5 + 100 mM KCl + 125 μM ferricyanide by increasing substrate concentration in the range 0−10 mM for L-lactate—inset1: calibration curve at E_{appl}: + 0.3 V by increasing substrate concentration in the range 0−10 mM for L-lactate—inset2: linear range of calibration curve for E-INK modified electrode; (D) effect of different pHs and temperature on E-INK modified electrode: 10 mM acetate buffer (black), 10 mM MOPS buffer (red)10 mM HEPES buffer (blue). Experimental conditions: 10 mM L-lactate, applied potential + 0.3 V; influence of interfering compounds on lactate response for E-INK modified electrode: 500 μM ascorbic acid, 500 μM dopamine, 500 μM glucose, 500 μM D-fructose, 500 μM D-mannitol, 500 μM D-galactose, 500 μM dopamine and 10 mM L-lactate measured with amperometry at E_{appl}: + 0.3 V and storage stability; (E) CVs for E-INK modified electrode in nonturnover (10 mM buffer pH = 7.5 + 100 mM KCl + 125 μM catechol, black curve) and turnover conditions (addition of 10 mM L-lactate, red curve), scan rate 5 mV s^{-1}; (F) amperometric measurements performed at E_{appl}: + 0.3 V for E-INK modified electrode in 10 mM buffer pH 7.5 + 100 mM KCl + 125 μM catechol by increasing substrate concentration in the range 0−10 mM for L-lactate—inset1: calibration curve at E_{appl}: + 0.3 V by increasing substrate concentration in the range 0−10 mM for L-lactate—inset2: linear range of calibration curve for E-INK modified electrode; (G) effect of different pHs and temperature on E-INK modified electrode: 10 mM acetate buffer (black), 10 mM MOPS buffer (red)10 mM HEPES buffer (blue). Experimental conditions: 10 mM L-lactate, applied potential + 0.3 V; Influence of interfering compounds on lactate response for E-INK modified electrode: 500 μM ascorbic acid, 500 μM glucose, 500 μM dopamine, 500 μM D-fructose, 500 μM D-mannitol, 500 μM D-galactose, 500 μM dopamine, and 10 mM L-lactate measured with amperometry at E_{appl}: + 0.3 V and storage stability.

https://doi.org/10.1021/acs.chemmater.3c02229
Chem. Mater. 2024, 36, 358−370

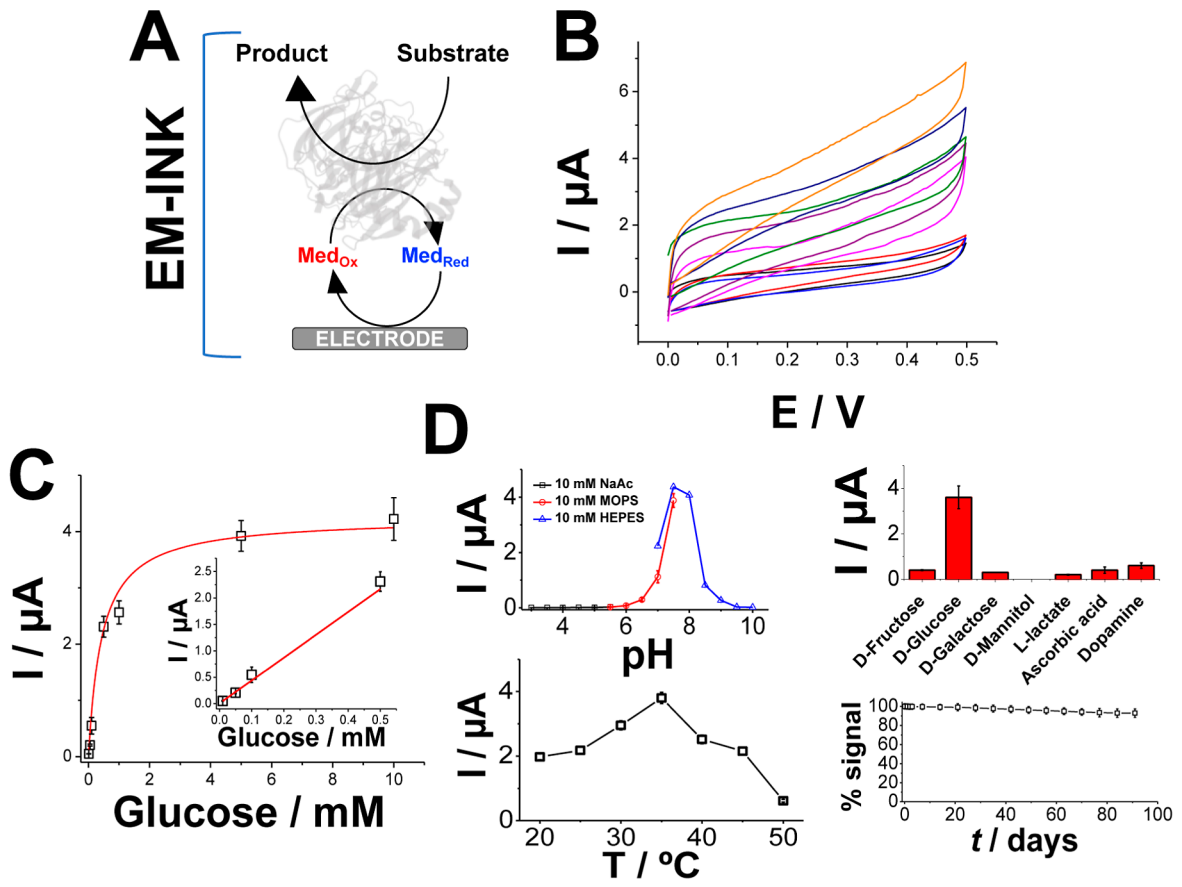

Figure 7. (A) Operating scheme of EM-INK; (B) CVs for EM-INK modified electrode in nonturnover (10 mM buffer pH 7.5 + 100 mM KCl, black curve) and turnover conditions (addition of different D-glucose concentrations up to 10 mM, colored curves), scan rate 5 mV s^{-1}; (C) calibration curve for EM-INK modified electrode in 10 mM buffer pH 7.5 + 100 mM KCl by increasing substrate concentration in the range 0−10 mM for D-glucose—inset: linear range of calibration curve for EM-INK modified electrode; (D) effect of different pHs and temperature on EM-INK modified electrode: 10 mM acetate buffer (black), 10 mM MOPS buffer (red)10 mM HEPES buffer (blue). Experimental conditions: 10 mM D-glucose, applied potential + 0.3 V; influence of interfering compounds on lactate response for EM-INK modified electrode: 500 μM ascorbic acid, 500 μM L-lactate, 500 μM dopamine, 500 μM D-fructose, 500 μM D-mannitol, 500 μM D-galactose, 500 μM dopamine, and 10 mM D-glucose measured with amperometry at E_{appl}: + 0.3 V and storage stability.

3.4. Comparison between Optimized Stencil-Printed Electrodes and Commercial Screen-Printed Electrodes. After obtaining the optimal ink formulation of 95% graphite and 1.5% chitosan (5.4 g of graphite, 0.3 mL of glycerol, and 9 mL of chitosan) based on DoE results, the optimized ink was used to stencil-print electrodes onto PET flexible supports. The so prepared electrodes were characterized using CV with 5 mM $Fe(CN)_6^{3-/4-}$ at various scan rates ranging from 5 to 150 mV s^{-1} (Figure 5A). The optimized electrodes reported an electroactive area (A_{EA}) of 3.95 ± 0.31 cm^2 using the Randles−Ševčík equation (Figure 5C). Considering a geometric area (A_{GEO}) of 0.09 cm^2, this results in a roughness factor (ρ) of 43.8. For comparison, a commercial screen-printed electrode was analyzed under similar conditions (CV with 5 mM $Fe(CN)_6^{3-/4-}$ at various scan rates ranging from 5 to 150 mV s^{-1}, Figure 5B) reporting an A_{EA} of 0.106 cm^2, which resulted in a roughness factor of 0.84 (considering its geometric area of 0.1256 cm^2). The low roughness factor might be ascribed to cracking effects due to high curing temperatures usually employed to fabricate screen-printed electrodes using organic solvents-based graphite inks. It should be highlighted that water-based inks are cured for shorter times and at lower temperatures avoiding the formation of cracks on electrode surfaces. Additionally, both electrodes were analyzed through EIS, as shown in Figure 5D. The optimized ink electrodes exhibited an R_{CT} of 9.6 ± 0.6 kΩ, which is 2.4 times lower than that of SPG electrodes (23.3 ± 1.3 kΩ). The extracted data from the fitting are reported in Table S2 (Supporting Information). This is in agreement with the results obtained by CVs and others previously reported.[16,18]

3.5. Enzyme-Based Inks for Printed Lactate and Glucose Flexible Biosensors. The optimized ink was further employed for the formulation of two different enzyme-based inks, namely, LOx modified optimized ink (referred to as enzyme-ink (E-INK), Figure 6A) and an ink containing both GOx and $[Os(4,4'\text{-dimethyl-}2,2'\text{-bipyridine})_2(\text{poly vinylimidazole})_{10}Cl]^{2+/+}$ (labeled as $[Os(dmbpy)_2(Cl)(PVI)_{10}]$) as redox mediator within the optimized graphite ink formulation (referred as EM-INK, Figure 7A).

To evaluate the catalytic behavior of the modified electrodes, several CV experiments were conducted in 10 mM HEPES buffer (pH 7 5) supplemented with 100 mM KCl, using 10 mM L-lactate and D-glucose as substrates, respectively. The E-INK printed electrodes were subjected to testing with two different diffusing redox mediators: ferricyanide (shown in Figure 6B−D) and catechol (shown in Figure 6E−G). Figure 6B illustrates the CVs obtained in the absence of substrates (black curve) and in the presence of 10 mM L-lactate (red

https://doi.org/10.1021/acs.chemmater.3c02229
Chem. Mater. 2024, 36, 358−370

curve). Under nonturnover conditions, particularly in the presence of 125 μM ferricyanide, the E-INK printed electrodes did not exhibit any redox peak, lacking any nonturnover redox activity. However, upon addition of the substrate, a catalytic curve emerged, starting at E_{ONSET} = + 0.165 V, and reaching a maximum current of 2 μA at E = + 0.4 V (Figure 6A, red curve). Similarly, Figure 6E presents the CVs in nonturnover (black curve) and turnover (red curve) conditions, with 125 μM catechol as the redox mediator. The CVs showed a catalytic curve starting at E_{ONSET} = + 0.182 V, with a maximum current of 3.7 μA at E = 0.4 V. The modified electrodes were further subjected to amperometry tests with increasing substrate concentrations ranging from 0 to 10 mM for L-lactate, as depicted in Figure 6C,E. The resulting calibration curves for the E-INK modified electrodes are shown in Figure 6C,E, covering a broad concentration range of 1×10^{-6} to 1×10^{-2} M. For the electrodes utilizing ferricyanide as the redox mediator, the calibration curve indicated a linear response within the range of 1−500 μM (as shown in Figure 6C, inset). The detection limit was found to be 0.3 ± 0.1 μM, and the sensitivity was calculated as 3.3 μA mM^{-1}. The correlation coefficient (R^2) for this calibration curve was 0.99, with a relative standard deviation (RSD) of 3.3% based on 10 measurements (n = 10). On the other hand, the electrodes employing catechol as the redox mediator displayed a linear response in the range of 10−500 μM (as shown in Figure 6E, inset). The detection limit was determined to be 3 ± 1 μM, and the sensitivity was calculated as 0.47 μA mM^{-1}. The correlation coefficient for this calibration curve was 0.97, with a RSD of 8.3% based on 10 measurements (n = 10). Additionally, both calibration curves were analyzed to derive classical Michaelis−Menten kinetic parameters. For ferricyanide as the mediator, the maximum current (I_{max}) was measured to be 3.7 ± 0.1 μA, and the apparent Michaelis−Menten constant (K_M^{app}) was determined to be 0.50 ± 0.05 mM. In the case of catechol as the mediator, the I_{max} was found to be 0.16 ± 0.01 μA, while the K_M^{app} was calculated as 0.23 ± 0.05 mM. The unexpected lower K_M^{app} values observed for the E-INK electrodes compared to literature values can be attributed to the altered diffusion coefficient of the substrate toward the enzyme-modified electrode, as well as the entrapment efficiency and orientation of the enzyme toward the graphite flakes within the ink.[52] These factors may influence the enzyme−substrate interaction and subsequently affect the apparent Michaelis−Menten constant. The effects of pH and temperature on the performance of the E-INK modified electrodes were also investigated for both ferricyanide and catechol as mediators. To cover a wide pH range between 3 and 10, three different buffers were used: acetate, MOPS, and HEPES buffers. The current signal showed an increase with increasing pH until reaching a maximum at pH 7.5 and thereafter decreasing as the pH was increased beyond 7.5. The optimal pH of 7.5 was consistent when using either of the two mediators (Figure 6D,G). Similarly, the temperature effect was assessed in 10 mM HEPES buffer at pH 7.5, supplemented with 100 mM KCl. The results revealed an optimum temperature range of 30−35 °C for the E-INK modified electrodes, which aligns with findings reported in the literature.[36] The selectivity of the E-INK modified electrodes was examined to evaluate the influence of the interfering compounds on their response. The signal obtained at a fixed concentration of L-lactate was compared to the signals obtained with equal amounts of various potential interfering compounds including D-fructose, D-galactose, D-mannitol, D-glucose, ascorbic acid, and dopamine. The results, as shown in Figure 6D,G, indicated that there was no significant current response for potential interfering compounds, except for ascorbic acid, which showed 11 and 9% interference in both cases. Ascorbic acid stands out among the other interferents due to its notably higher diffusion coefficient ($D = 5.9 \times 10^{-6}$ cm^2 s^{-1}) and ease of oxidation at the electrode surface, especially at the applied potential utilized for these analytical measurements. This ease of oxidation can lead to interference in electrochemical measurements, causing detectable signals in the presence of ascorbic acid. Additionally, the storage stability of the E-INK modified electrodes was investigated by subjecting electrodes to 10 measurements every day over a 90-day period using a 10 mM L-lactate solution. The results, as reported in Figure 6D,G, indicated that the E-INK modified electrodes exhibited a signal decrease of less than 15−20% of their initial response after 90 days of continuous use. This observed stability can be attributed to a combination of factors, including the intrinsic stability of the enzyme enclosed within the formulated ink, ink deposition, and homogeneity.

Similarly, the enzyme mediator-ink (EM-INK) printed electrodes were tested as reported in Figure 7A−C. Figure 7B depicts the CVs obtained in the absence of substrate (black curve) and in the presence of D-glucose from 10 μM to 10 mM (colored curves). Under nonturnover conditions, the EM-INK printed electrodes did not exhibit any redox peak, indicating a limited nonturnover redox activity. However, upon addition of the substrate, catalytic current is observed starting at E_{ONSET} = 0 V. The resulting calibration curve for the EM-INK modified electrodes are shown in Figure 7C, covering a broad concentration range of 1×10^{-6} to 1×10^{-2} M. The calibration curve indicated a linear response within the range of 10−500 μM (as shown in Figure 7B, inset). The detection limit was found to be 3 ± 1 μM, and the sensitivity was calculated as 4.3 μA mM^{-1}. The correlation coefficient (R^2) for this calibration curve was 0.99, with a RSD of 4.2% based on 10 measurements (n = 10). Additionally, the calibration curve was analyzed to derive the classical Michaelis−Menten kinetic parameters. For the ORP as the mediator, the maximum current (I_{max}) was measured to be 4.3 ± 0.3 μA, and the apparent Michaelis−Menten constant (K_M^{app}) was determined to be 0.4 ± 0.1 mM. The lower K_M^{app} values observed for the EM-INK electrodes can indeed be attributed to several factors, including the altered diffusion coefficient of the substrate toward the enzyme-modified electrode, as well as the entrapment efficiency and orientation of the enzyme within the graphite flakes of the ink.[52] These factors can affect the accessibility of the substrate to the active sites of the enzyme, influencing the enzyme−substrate interaction and, consequently, affecting the apparent Michaelis−Menten constant (K_M^{app}). The effects of pH and temperature on the EM-INK modified electrodes (Figure 7D) were evaluated, showing a maximum current signal at pH 7.5, which corresponds to the maximum current signal obtained in HEPES buffer. The optimum temperature (Figure 7D) was found to be 30−35 °C, in agreement with the literature.[3] The selectivity of the EM-INK modified electrodes was studied to assess the interfering compounds' influence on its response. Interference tests with various compounds showed no significant current responses, except for ascorbic acid, which exhibited a higher diffusion coefficient and ease of oxidation at the electrode surface. The storage stability of the EM-INK modified electrodes (Figure

https://doi.org/10.1021/acs.chemmater.3c02229
Chem. Mater. 2024, 36, 358−370

7D) was investigated, showing a signal decrease of less than 10% after 90 days of daily use for a 10 mM D-glucose solution, possibly attributed to the enzyme intrinsic stability enclosed within the formulated ink.

4. CONCLUSIONS

This work reports a novel approach based on a rational design to formulate water-based graphite conductive inks integrating enzymes and electron transfer mediators to obtain fully printed highly performing enzyme-based amperometric biosensors for lactate and glucose detection. Noteworthy the stencil-printed electrodes displayed an electroactive area (A_{EA}) of 3.95 ± 0.31 cm^2 and a roughness factor (ρ) of 43.8, a value 50 times higher than commercially available screen-printed electrodes. Additionally, the incorporation of lactate oxidase and GOx within water-based graphite conductive ink led to the creation of enzyme-based inks, termed E-INK for lactate detection and EM-INK for glucose detection. The resultant biosensors showcased remarkable sensitivity and a low LOD, measuring 3.3 $\mu A\ mM^{-1}$ and 0.3 ± 0.1 μM (utilizing ferricyanide as an electron mediator) and 0.47 $\mu A\ mM^{-1}$ and 3 ± 1 μM (utilizing catechol as an electron mediator) for E-INK, and 4.3 $\mu A\ mM^{-1}$ and 3 ± 1 μM for EM-INK. Notably, these biosensors also exhibited exceptional selectivity and maintained their storage stability, retaining approximately 80−90% of the initial signal even after 90 days. The suggested system exhibits encouraging characteristics that make it suitable for use as a versatile, wearable biosensor. It utilizes biocompatible water-based inks, making it potentially applicable in sports medicine and remote clinical care settings. Moreover, there is potential for further development, leading to the creation of edible biosensors capable of continuously monitoring metabolites.

■ ASSOCIATED CONTENT

Supporting Information

The Supporting Information is available free of charge at https://pubs.acs.org/doi/10.1021/acs.chemmater.3c02229.

EIS data extracted for run #1 to run #11. Table S2 EIS data extracted for the optimized ink compared with the commercial SPEb (PDF)

■ AUTHOR INFORMATION

Corresponding Authors

Luisa Torsi − *Department of Chemistry, University of Bari Aldo Moro, Bari 70125, Italy; Centre for Colloid and Surface Science, University of Bari Aldo Moro, Bari 70125, Italy;* orcid.org/0000-0002-0798-0780; Email: luisa.torsi@uniba.it

Paolo Bollella − *Department of Chemistry, University of Bari Aldo Moro, Bari 70125, Italy; Centre for Colloid and Surface Science, University of Bari Aldo Moro, Bari 70125, Italy;* Email: paolo.bollella@uniba.it

Eleonora Macchia − *Centre for Colloid and Surface Science and Department of Pharmacy-Pharmaceutical Sciences, University of Bari Aldo Moro, Bari 70125, Italy; Faculty of Science and Engineering, Åbo Akademi University, Turku 20500, Finland;* orcid.org/0000-0002-1534-7336; Email: eleonora.macchia@uniba.it

Authors

Verdiana Marchianò − *Department of Chemistry, University of Bari Aldo Moro, Bari 70125, Italy; Centre for Colloid and Surface Science, University of Bari Aldo Moro, Bari 70125, Italy*

Angelo Tricase − *Department of Chemistry, University of Bari Aldo Moro, Bari 70125, Italy; Centre for Colloid and Surface Science, University of Bari Aldo Moro, Bari 70125, Italy*

Mariapia Caputo − *Department of Pharmacy-Pharmaceutical Sciences, University of Bari Aldo Moro, 70125 Bari, Italy*

Emanuele Farinini − *Department of Pharmacy, University of Genoa, Genoa 16148, Italy*

Riccardo Leardi − *Department of Pharmacy, University of Genoa, Genoa 16148, Italy*

Anna Imbriano − *Department of Chemistry, University of Bari Aldo Moro, Bari 70125, Italy; Centre for Colloid and Surface Science, University of Bari Aldo Moro, Bari 70125, Italy*

Dónal Leech − *School of Biological & Chemical Sciences, University of Galway, Galway H91 TK33, Ireland;* orcid.org/0000-0001-7844-1306

Reshma Kidayaveettil − *School of Biological & Chemical Sciences, University of Galway, Galway H91 TK33, Ireland;* orcid.org/0000-0001-8907-9285

Luigi Gentile − *Department of Chemistry, University of Bari Aldo Moro, Bari 70125, Italy; Centre for Colloid and Surface Science, University of Bari Aldo Moro, Bari 70125, Italy;* orcid.org/0000-0001-6854-2963

Complete contact information is available at: https://pubs.acs.org/10.1021/acs.chemmater.3c02229

Author Contributions

P.B., E.M., L.G., and L.T. conceived the project and wrote the manuscript. V.M., A.T., M.C., and A.I. performed all electrochemical measurements. L.G. performed the rheological characterizations and related data analysis. R.K. synthesized the ORPs. D.L. supervised R.K. E.F. and R.L. supported the use of CAT software for DoE analysis. E.M. conceived the DoE. L.T., P.B., and E.M. directly supervised V.M., A.T., M.C., and A.I. during the project. D.L. L.T., E.M., P.B., R.L., and E.F. revised the manuscript. L.T., E.M., P.B., and D.L. are responsible for funding acquisition. The final version was approved by all authors.

Notes

The authors declare no competing financial interest.

■ ACKNOWLEDGMENTS

The following funding agencies are acknowledged: Academy of Finland projects #316881, #316883 "Spatiotemporal control of Cell Functions", #332106 "ProSiT—Protein Detection at the Single-Molecule Limit with a Self-powered Organic Transistor for HIV early diagnosis"; Biosensori analitici usa-e getta a base di transistori organici autoalimentati per la rivelazione di biomarcatori proteomici alla singola molecola per la diagnostic decentrata dell'HIV (6CDD3786); Research for Innovation REFIN—Regione Puglia POR PUGLIA FESR-FSE 2014/2020; PMGBARS01_01195; NoOne-A binary sensor with single-molecule digit to discriminate biofluids enclosing zero or at least one biomarker, ERC Stg2021, GA:101040383; PRIN project prot.2017RHX2E4 "At the forefront of Analytical ChemisTry: disrUptive detection technoLogies to improve food safety—ACTUaL"; IDF SHARID (ARS01_01270); ÅboAkademi University CoE "Bioelectronic activation of cell functions"; University of Galway College of Science and Engineering Scholarship and CSGI are acknowledged for partial financial support.

REFERENCES

(1) Bollella, P. Enzyme-Based Amperometric Biosensors: 60 Years Later··· Quo Vadis? *Anal. Chim. Acta* **2022**, *1234*, 340517.
(2) Kim, J.; Campbell, A. S.; de Ávila, B. E. F.; Wang, J. Wearable Biosensors for Healthcare Monitoring. *Nat. Biotechnol.* **2019**, *37* (4), 389−406.
(3) Wang, J. Electrochemical Glucose Biosensors. *Chem. Rev.* **2008**, *108* (2), 814−825.
(4) Battista, E.; Lettera, V.; Villani, M.; Calestani, D.; Gentile, F.; Netti, P. A.; Iannotta, S.; Zappettini, A.; Coppede, N. Enzymatic Sensing with Laccase-Functionalized Textile Organic Biosensors. *Org. Electron.* **2017**, *40*, 51−57.
(5) Bollella, P. Porous Gold: A New Frontier for Enzyme-Based Electrodes. *Nanomaterials* **2020**, *10* (4), 722.
(6) Shiwaku, R.; Matsui, H.; Nagamine, K.; Uematsu, M.; Mano, T.; Maruyama, Y.; Nomura, A.; Tsuchiya, K.; Hayasaka, K.; Takeda, Y.; et al. A Printed Organic Circuit System for Wearable Amperometric Electrochemical Sensors. *Sci. Rep.* **2018**, *8* (1), 6368.
(7) Sardini, E.; Serpelloni, M.; Tonello, S. Printed Electrochemical Biosensors: Opportunities and Metrological Challenges. *Biosensors* **2020**, *10* (11), 166.
(8) Elbadawi, M.; Ong, J. J.; Pollard, T. D.; Gaisford, S.; Basit, A. W. Additive Manufacturable Materials for Electrochemical Biosensor Electrodes. *Adv. Funct. Mater.* **2021**, *31* (10), 2006407.
(9) Wang, J.; Musameh, M. Carbon Nanotube Screen-Printed Electrochemical Sensors. *Analyst* **2004**, *129* (1), 1−2.
(10) Bolon: UV Radiation curable electrically conductive··· - Google Scholar. https://scholar.google.com/scholar_lookup?title=UVRadiationCurableElectricallyConductiveInkandCircuitBoardsMadeTherewith&publication_year=1978&author=D.A.Bolon&author=G.M.Lucas&author=S.H.Schroeter (accessed Feb 23, 2023).
(11) Dimitriou, E.; Michailidis, N. Printable Conductive Inks Used for the Fabrication of Electronics: An Overview. *Nanotechnology* **2021**, *32* (50), 502009.
(12) Camargo, J. R.; Orzari, L. O.; Araujo, D. A. G.; de Oliveira, P. R.; Kalinke, C.; Rocha, D. P.; Luiz dos Santos, A.; Takeuchi, R. M.; Munoz, R. A. A.; Bonacin, J. A.; et al. Development of Conductive Inks for Electrochemical Sensors and Biosensors. *Microchem. J.* **2021**, *164*, 105998.
(13) Kn, H. P.; Cs, M.; Karunakar Raju, N.; Sp, S.; Mr, Y.; Manjunatha, C. Current Developments in Conductive Nano-Inks for Flexible and Wearable Electronics. *ECS Trans.* **2022**, *107* (1), 11261−11275.
(14) Gevaerd, A.; Watanabe, E. Y.; Belli, C.; Marcolino-Junior, L. H.; Bergamini, M. F. A Complete Lab-Made Point of Care Device for Non-Immunological Electrochemical Determination of Cortisol Levels in Salivary Samples. *Sens. Actuators, B* **2021**, *332*, 129532.
(15) Araujo, D. A.; Camargo, J. R.; Pradela-Filho, L. A.; Lima, A. P.; Munoz, R. A.; Takeuchi, R. M.; Janegitz, B. C.; Santos, A. L. A Lab-Made Screen-Printed Electrode as a Platform to Study the Effect of the Size and Functionalization of Carbon Nanotubes on the Voltammetric Determination of Caffeic Acid. *Microchem. J.* **2020**, *158*, 105297.
(16) Camargo, J. R.; Silva, T. A.; Rivas, G. A.; Janegitz, B. C. Novel Eco-Friendly Water-Based Conductive Ink for the Preparation of Disposable Screen-Printed Electrodes for Sensing and Biosensing Applications. *Electrochim. Acta* **2022**, *409*, 139968.
(17) Aleeva, Y.; Pignataro, B. Recent Advances in Upscalable Wet Methods and Ink Formulations for Printed Electronics. *J. Mater. Chem. C* **2014**, *2* (32), 6436−6453.
(18) Tricase, A.; Imbriano, A.; Valentino, M.; Ditaranto, N.; Macchia, E.; Franco, C. D.; Kidayaveettil, R.; Leech, D.; Piscitelli, M.; Scamarcio, G.; Perchiazzi, G.; Torsi, L.; Bollella, P. Water-Based Conductive Ink Formulations for Enzyme-Based Wearable Biosensors. *Adv. Sens. Res.* **2023**, *2*, 2300036.
(19) Silveri, F.; Paolini, D.; Della Pelle, F.; Bollella, P.; Scroccarello, A.; Suzuki, Y.; Fukawa, E.; Sowa, K.; Di Franco, C.; Torsi, L.; Compagnone, D. Lab-Made Flexible Third-Generation Fructose Biosensors Based on 0D-Nanostructured Transducers. *Biosens. Bioelectron.* **2023**, *237*, 115450.
(20) Hasegawa, N.; Kamiya, A.; Matsunaga, T.; Kitano, N.; Harada, M. Analysis of Crack Formation during Fuel Cell Catalyst Ink Drying Process. Reduction of Catalyst Layer Cracking by Addition of High Boiling Point Solvent. *Colloids Surf., A* **2021**, *628*, 127153.
(21) Bonnassieux, Y.; Brabec, C. J.; Cao, Y.; Carmichael, T. B.; Chabinyc, M. L.; Cheng, K.-T.; Cho, G.; Chung, A.; Cobb, C. L.; Distler, A.; et al. The 2021 Flexible and Printed Electronics Roadmap. *Flexible Printed Electron.* **2021**, *6* (2), 023001.
(22) Sempionatto, J. R.; Montiel, V. R.-V.; Vargas, E.; Teymourian, H.; Wang, J. Wearable and Mobile Sensors for Personalized Nutrition. *ACS Sens.* **2021**, *6* (5), 1745−1760.
(23) Sempionatto, J. R.; Lasalde-Ramírez, J. A.; Mahato, K.; Wang, J.; Gao, W. Wearable Chemical Sensors for Biomarker Discovery in the Omics Era. *Nat. Rev. Chem* **2022**, *6*, 899−915.
(24) Min, J.; Sempionatto, J. R.; Teymourian, H.; Wang, J.; Gao, W. Wearable Electrochemical Biosensors in North America. *Biosens. Bioelectron.* **2021**, *172*, 112750.
(25) Van Hoovels, K.; Xuan, X.; Cuartero, M.; Gijssel, M.; Swarén, M.; Crespo, G. A. Can Wearable Sweat Lactate Sensors Contribute to Sports Physiology? *ACS Sens.* **2021**, *6* (10), 3496−3508.
(26) Ye, J.; Chu, T.; Chu, J.; Gao, B.; He, B. A Versatile Approach for Enzyme Immobilization Using Chemically Modified 3D-Printed Scaffolds. *ACS Sustain. Chem. Eng.* **2019**, *7* (21), 18048−18054.
(27) Schmieg, B.; Döbber, J.; Kirschhöfer, F.; Pohl, M.; Franzreb, M. Advantages of Hydrogel-Based 3D-Printed Enzyme Reactors and Their Limitations for Biocatalysis. *Front. Bioeng. Biotechnol.* **2019**, *6*, 211.
(28) Lyons, M. E. G.; Greer, J. C.; Fitzgerald, C. A.; Bannon, T.; Barlett, P. N. Reaction/Diffusion with Michaelis-Menten Kinetics in Electroactive Polymer Films. Part 1. The Steady-State Amperometric Response. *Analyst* **1996**, *121* (6), 715−731.
(29) Bollella, P.; Gorton, L. Enzyme Based Amperometric Biosensors. *Curr. Opin. Electrochem.* **2018**, *10*, 157−173.
(30) Bollella, P.; Katz, E. Enzyme-Based Biosensors: Tackling Electron Transfer Issues. *Sensors* **2020**, *20* (12), 3517.
(31) Adachi, T.; Kitazumi, Y.; Shirai, O.; Kano, K. Direct Electron Transfer-Type Bioelectrocatalysis of Redox Enzymes at Nanostructured Electrodes. *Catalysts* **2020**, *10* (2), 236.
(32) Lisdat, F. *Biosensing for the 21st Century*; Springer, 2007; Vol. *109*.
(33) Lisdat, F. PQQ-GDH-Structure, Function and Application in Bioelectrochemistry. *Bioelectrochemistry* **2020**, *134*, 107496.
(34) Gorton, L. *Special Issue on Sugar Oxidising Enzymes*; Elsevier, 2020.
(35) Leiros, I.; Wang, E.; Rasmussen, T.; Oksanen, E.; Repo, H.; Petersen, S. B.; Heikinheimo, P.; Hough, E. The 2.1 Å Structure of Aerococcus Viridans L-Lactate Oxidase (LOX). *Acta Crystallogr., Sect. F: Struct. Biol. Cryst. Commun.* **2006**, *62* (12), 1185−1190.
(36) Biryukova, E. N.; Arinbasarova, A. Y.; Medentsev, A. G. L-Lactate Oxidase Systems of Microorganisms. *Microbiology* **2022**, *91* (2), 124−132.
(37) Bankar, S. B.; Bule, M. V.; Singhal, R. S.; Ananthanarayan, L. Glucose Oxidase—an Overview. *Biotechnol. Adv.* **2009**, *27* (4), 489−501.
(38) Bartlett, P. N.; Al-Lolage, F. A. There Is No Evidence to Support Literature Claims of Direct Electron Transfer (DET) for Native Glucose Oxidase (GOx) at Carbon Nanotubes or Graphene. *J. Electroanal. Chem.* **2018**, *819*, 26−37.
(39) Wilson, G. S. Native Glucose Oxidase Does Not Undergo Direct Electron Transfer. *Biosens. Bioelectron.* **2016**, *82*, vii−viii.
(40) Samadi, N.; Aberoomand Azar, P.; Waqif Husain, S.; Maibach, H. I.; Nafisi, S. Experimental Design in Formulation Optimization of Vitamin K1 Oxide-Loaded Nanoliposomes for Skin Delivery. *Int. J. Pharm.* **2020**, *579*, 119136.
(41) Leardi, R. Experimental Design in Chemistry: A Tutorial. *Anal. Chim. Acta* **2009**, *652* (1−2), 161−172.

https://doi.org/10.1021/acs.chemmater.3c02229
Chem. Mater. 2024, 36, 358−370

(42) Scandurra, C.; Bollella, P.; Österbacka, R.; Leonetti, F.; Macchia, E.; Torsi, L. Implementation of Experimental Design Techniques to Optimize Immunoglobulins Detection with Ultrasensitive Sandwich Immunoassays. *Adv. Sens. Res.* **2022**, *1* (1), 2200009.
(43) Scandurra, C.; Björkström, K.; Sarcina, L.; Imbriano, A.; Di Franco, C.; Österbacka, R.; Bollella, P.; Scamarcio, G.; Torsi, L.; Macchia, E. Single Molecule with a Large Transistor-SiMoT Cytokine IL-6 Detection Benchmarked against a Chemiluminescent Ultrasensitive Immunoassay Array. *Adv. Mater. Technol.* **2023**, *8* (11), 2201910.
(44) Jayakumar, K.; Bennett, R.; Leech, D. Electrochemical Glucose Biosensor Based on an Osmium Redox Polymer and Glucose Oxidase Grafted to Carbon Nanotubes: A Design-of-Experiments Optimisation of Current Density and Stability. *Electrochim. Acta* **2021**, *371*, 137845.
(45) Gentile, L.; Amin, S.Rheology Primer for Nanoparticle Scientists. In *Colloidal Foundations of Nanoscience*; Elsevier, Berti, D., Palazzo, P., 2nd Ed., 2022; 289306.
(46) Leardi, R.; Melzi, C.; Polotti, G. M. CAT (Chemometric Agile Tool), Freely downloadable from https://gruppochemiometria.it/index.php/software (accessed on Aug 31, 2023).
(47) Paixão, T. R. L. C. Measuring Electrochemical Surface Area of Nanomaterials versus the Randles- Ševčík Equation. *ChemElectroChem* **2020**, *7* (16), 3414−3415.
(48) Lavagnini, I.; Antiochia, R.; Magno, F. An Extended Method for the Practical Evaluation of the Standard Rate Constant from Cyclic Voltammetric Data. *Electroanalysis* **2004**, *16* (6), 505−506.
(49) Glasser, A.; Cloutet, E.; Hadziioannou, G.; Kellay, H. Tuning the Rheology of Conducting Polymer Inks for Various Deposition Processes. *Chem. Mater.* **2019**, *31* (17), 6936−6944.
(50) Vachoud, L.; Zydowicz, N.; Domard, A. Physicochemical Behaviour of Chitin Gels. *Carbohydr. Res.* **2000**, *326* (4), 295−304.
(51) Tatini, D.; Tempesti, P.; Ridi, F.; Fratini, E.; Bonini, M.; Baglioni, P. Pluronic/Gelatin Composites for Controlled Release of Actives. *Colloids Surf., B* **2015**, *135*, 400−407.
(52) Xu, P.; Yano, T.; Yamamoto, K.; Suzuki, H.; Kumagai, H. Characterization of a Lactate Oxidase from a Strain of Gram Negative Bacterium from Soil. *Appl. Biochem. Biotechnol.* **1996**, *56* (3), 277−288.

https://doi.org/10.1021/acs.chemmater.3c02229
Chem. Mater. 2024, 36, 358−370